Eur. Phys. J. B (2012) 85: 312
DOI: 10.1140/epjb/e2012-30148-5

THE EUROPEAN PHYSICAL JOURNAL B

Regular Article

Study of direct and indirect exciton states in GaAs-$Ga_{1-x}Al_xAs$ quantum dots under the effects of intense laser field and applied electric field

M.E. Mora-Ramos[1], C.A. Duque[2,a], E. Kasapoglu[3], H. Sari[3], and I. Sökmen[4]

[1] Facultad de Ciencias, Universidad Autónoma del Estado de Morelos, avenida Universidad 1001, CP 62209, Cuernavaca, Morelos, Mexico
[2] Instituto de Física, Universidad de Antioquia, AA 1226, Medellín, Colombia
[3] Cumhuriyet University, Physics Department, 58140 Sivas, Turkey
[4] Dokuz Eylül University, Physics Department, 35160 Buca, İzmir, Turkey

Received 18 February 2012 / Received in final form 2 June 2012
Published online 12 September 2012 –

Abstract. The effects of intense laser radiation on the exciton states in GaAs-$Ga_{1-x}Al_xAs$ quantum dots are studied with the inclusion of applied dc electric fields oriented along the growth direction of the system. The calculations are made within the effective mass and parabolic band approximations. The intense laser effects have been included along the lines of the Floquet method, modifying the confinement potential associated to the heterostructure. The laser field modifies the Coulomb potential via the generation of two interaction centers. The exciton binding energy behaves as a decreasing function of the laser field strength, as well as of the size of the quantum dot. The normalized photoluminescence peak energy increases with the laser field strength and behaves as a decreasing function of the dot's dimensions for fixed laser field intensity.

1 Introduction

The electron and hole states in nanostructures are affected by the application of electric and/or magnetic fields, and also by external perturbations like hydrostatic pressure or temperature [1]. On the other hand, the evolution of the emerging field of nanoelectronics is closely related to the study of the effects of external electromagnetic fields on the optical and transport properties of low-dimensional systems [2].

The realization of research activities on the interaction of intense laser fields (ILF) with carriers in semiconductor nanostructures was stimulated by the development of high-power tunable laser sources, such as free electron lasers [3]. Within this context, several interesting physical phenomena have been revealed. We can mention, for instance, the presence of changes in the electron density of states in quantum wells (QWs) and quantum well wires (QWWs) [4–6], the measurement of zero-resistance states in two-dimensional electron gases under microwave radiation [7], terahertz resonant absorption in QWs [8], and Floquet-Bloch states in single-walled carbon nanotubes [9], among others.

The influence of an intense high-frequency laser field on different physical properties of bulk semiconductors has received some discussion and analysis in the literature [10–13]. A number of investigations on the effect of laser fields on low dimensional heterostructures have been published. The dressed atom approach was extended by Brandi et al. [14,15] to treat the influence of the laser field upon a semiconductor system. The interaction with the laser enters in the calculation via the renormalization of the semiconductor effective mass. More recently, a theoretical study of the combined effects of intense high frequency laser and static magnetic fields on the binding and transition energies was developed by Niculescu et al. to investigate the ground and some excited states of an on-center hydrogenic donor in a cylindrical GaAs QWW [16]. As an outcome, the effect of the laser field reveals to be more pronounced for s-like states, whereas for $2p$-like states the binding energy is weakly dependent on the laser dressing parameter. Within the same scheme, one also finds the report on the laser-dressing effects on the electron g-factor in GaAs-$Ga_{1-x}Al_xAs$ QWs and QWWs under applied magnetic fields [17]. The possibility of manipulating and tuning the conduction-electron g-factor in heterostructures by changing the detuning and laser field intensity was discussed in that work.

Furthermore, the ILF effects on the density of impurity states of shallow donors in a square, V-shaped, and inverse V-shaped QWs have been studied by Niculescu et al. [18,19]. It was concluded that a proper consideration

[a] e-mail: cduque_echeverri@yahoo.es

of the density of impurity states may be relevant in the interpretation of the optical phenomena associated with shallow impurities in QWs; where there is a competition between the effects of an ILF, the applied dc electric field and the quantum confinement. The laser effects have also been included in calculations of a donor-impurity polarizability in a QW under an applied electric field, with the finding of a lack of monotonicity for the polarizability as a function of external perturbations like an applied electric field and the incoming laser radiation [20].

It is also possible to mention some very recent studies regarding the ILF effects on the optical properties of semiconducting nanostructures. In this sense, there is a report concerning the THz laser field effects on the oscillator strength and the linear and nonlinear refractive index changes in cylindrical QWWs [21]. Besides, an investigation on the anisotropic optical absorption in QWWs, induced by high-frequency laser fields has been also put forward [22].

The appearance of an unexpected transition from single to double QW potential induced by ILF was revealed in a theoretical study from Lima et al. [23]. Using the laser-dressed potential model in single QWs, the authors have found the formation of a double-well potential structure in the regime $\alpha_0 > L/2$, where L is the QW width and α_0 is the laser-dressing parameter. This fact is associated with the possibility of generating resonant states into the system's channel, as well as of controlling the population inversion in QW lasers operating in the optical pumping scheme. Finally, the study of ILF effects has been extended to other heterostructures such as QWWs and QDs with several configurations of the quantum confinement, stoichiometry of the well and barrier regions, geometries of the systems, and external perturbations like applied electric and magnetic fields and hydrostatic pressure [24–27].

The knowledge of exciton states is important for the correct understanding of some optical properties in the semiconducting low-dimensional systems. Therefore, the investigation of the excitonic properties in heterostructures under ILF is, arguably, an area of current interest. Accordingly, the present work is concerned with the theoretical study of the effects of ILF on the exciton states in single QDs. The research is extended to include the additional influence of an applied dc electric field oriented along the growth direction. The laser-dressed potential above mentioned, as well as the effect of single-to-double potential well transition are the subject of particular investigation in our case. The paper is organized as follows. In Section 2 we describe the theoretical framework. Section 3 is dedicated to the results and discussion, and finally, our conclusions are given in Section 4.

2 Theoretical framework

We are concerned here with the effects of ILF on the binding energy of a heavy-hole exciton in a GaAs-$Ga_{1-x}Al_xAs$ QD of cylindrical shape, grown along the z-axis and in the presence of applied electric field. The calculation assumes the envelope-function and parabolic-band approximations. The choice for the electric field orientation is $\vec{F} = (0, 0, -F)$.

In order to provide a simpler description of the main equations in the theoretical approach, we use effective units. That is, we express energies in effective Rydberg $\left(R_0 = \frac{\mu\, e^4}{2\,\hbar^2\,\varepsilon_0^2}\right)$ and lengths in effective Bohr radius $\left(a_0^* = \frac{\hbar^2\,\varepsilon_0}{\mu\, e^2}\right)$. According to the model proposed by Le Goff and Stébé, the Hamiltonian for the exciton states in a cylindrical GaAs-$Ga_{1-x}Al_xAs$ QD under in-growth direction applied electric field is given by [28]:

$$H = \sum_{i=e,h} \left\{ -\frac{\mu}{m_i^*}\left[\frac{\partial^2}{\partial\rho_i^2} + \frac{1}{\rho_i}\frac{\partial}{\partial\rho_i} + \frac{\rho^2 \pm (\rho_e^2 - \rho_h^2)}{\rho\,\rho_i}\frac{\partial^2}{\partial\rho\,\partial\rho_i}\right] - \frac{\mu}{m_i^*}\frac{\partial^2}{\partial z_i^2} + V_i(\rho_i, z_i) \pm e\,F\,z_i \right\} - \left[\frac{\partial^2}{\partial\rho^2} + \frac{1}{\rho}\frac{\partial}{\partial\rho}\right] - \frac{2}{r}, \quad (1)$$

where $r = \sqrt{\rho^2 + (z_e - z_h)^2}$, $\rho = |\overrightarrow{\rho_e} - \overrightarrow{\rho_h}|$, and $\pm$ stands for electrons and holes, respectively. In addition, m_e^* (m_h^*) labels electron (hole) effective mass, while μ is the electron-hole reduced mass, e is the electron charge, ε_0 is the GaAs static dielectric constant, and $V_e(\rho_e, z_e)$ [$V_h(\rho_h, z_h)$] is the QD confinement potential for the electron (hole) carrier.

Our model considers the dimensions of the cylindrical QD to be labeled as: radius, R, and height, L. For the confinement potential of the carriers we have taken into account infinite and finite confinement potentials in the ρ- and z-directions, respectively (see Figs. 1c and 1d). Within such an approximation it is valid to perform the separation $V_i(\rho_i, z_i) = V_i^{\rho}(\rho_i) + V_i^{z}(z_i)$. Here $V_i^{\rho}(\rho_i) = 0$ for $\rho_i \leq R$ and $V_i^{\rho}(\rho_i) \to \infty$ for $\rho_i > R$. In the case of the z-dependent confinement we have $V_i^z(z_i) = 0$ for $|z_i| \leq L/2$ and $V_i^z(z_i) = V_0^i$ for $|z_i| > L/2$. For electrons (holes) the height of axial confinement potential V_0^e (V_0^h) follows from the offset rule that sets 60% (40%) of the band gap between the well (GaAs) and barrier ($Ga_{1-x}Al_xAs$) materials.

In order to include the non-resonant ILF effects (the polarization of the laser radiation is parallel to the z-direction), the so-called Floquet method is adopted [29,30]. According to this formalism, the single particle z_i-dependent confinement potentials must be replaced by $V_i^z(z_i) \to \langle V_i^z\rangle(z_i, \alpha_{0i})$ as follows:

$$\langle V_i^z\rangle(z_i, \alpha_{0i}) = \frac{V_0^i}{\pi}\left[\Theta(\alpha_{0i} - z_i - L/2)\,\arccos\left(\frac{L/2 + z_i}{\alpha_{0i}}\right) + \Theta(\alpha_{0i} + z_i - L/2)\,\arccos\left(\frac{L/2 - z_i}{\alpha_{0i}}\right)\right], \quad (2)$$

where

$$\alpha_{0i} = (e\,A_0)/(m_i^*\,c\,\omega) = (I^{1/2}/\omega^2)(e/m_i^*)(8\,\pi/c)^{1/2}, \quad (3)$$

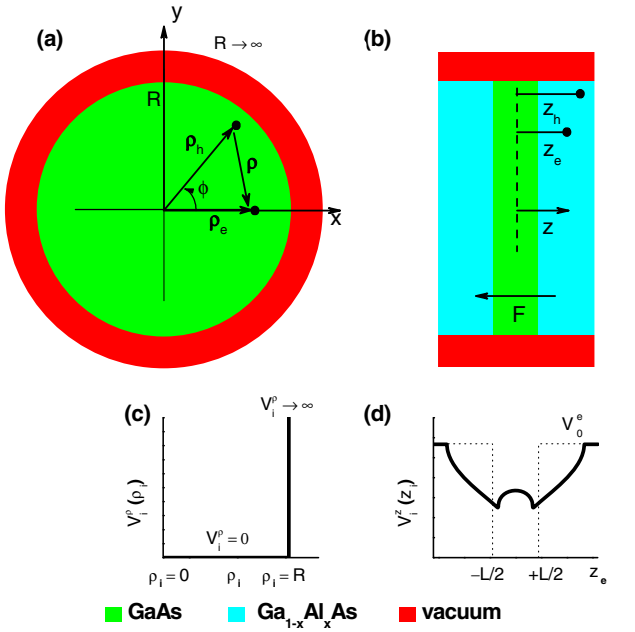

Fig. 1. (Color online) Pictorial view of the cylindrical quantum dot considered in the present work. Graphs (a) and (b) show, respectively, the xy and xz projections, defining the dimensions of the heterostructure, the directions of the applied electric field, and the electron and hole positions. Schematic representations of the radial (ρ) and axial (z) confinement potentials are depicted in (c) and (d), respectively. In (d) the confinement potential corresponds particularly to the electron one with $\alpha_{0e} = L$.

is the laser-dressing parameter (from now on ILF-parameter) [31]. In equation (3), I and ω are, respectively, the average intensity and the frequency of the laser, c is the velocity of the light, and A_0 is the amplitude of the vector potential associated with the incident radiation.

Under the laser effects the last term of equation (1) – the one-center electron-hole Coulomb interaction – must be replaced by a two-center Coulomb interaction as

$$\langle V\rangle_C(z_e, z_h, \alpha_0) = -\frac{1}{[\rho^2 + (z_{eh} - \alpha_0)^2]^{1/2}} - \frac{1}{[\rho^2 + (z_{eh} + \alpha_0)^2]^{1/2}}, \quad (4)$$

where $z_{eh} = z_e - z_h$ and $\alpha_0 = (e\,A_0)/(\mu\,c\,\omega)$. Extended details about dressed potential in equations (2) and (4) and the nonperturbative theory developed to describe the atomic behavior in intense high frequency laser field can be found in references [22,23,32–35].

In the laser regime in which $\alpha_{0i} > L/2$ it clearly exists a spatial region along the z direction where the contributions coming from the two terms at the right hand side of equation (2) superpose. This means that the influence of the laser field produces an interaction between the two potential barriers locates at $\pm L/2$. As a result, a well pronounced maximum of the potential appears in the vicinity of $z = 0$ which, in our study, corresponds to a potential barrier that uncouples a pair of symmetric dots. This fact gives rise to the double quantum well system (see. Fig. 1d). In addition, due to the presence of the two inverse cosine functions in equation (2) – shifted in $\pm L/2$–, it comes out that the potential barriers show a decreasing/increasing value when the argument goes from/to $-L/2 - \alpha_{0i}/+L/2 + \alpha_{0i}$ which reflects in an increment of the effective quantum well width from L to $L + 2\,\alpha_{0i}$ (see Fig. 1d).

The exciton wave function, and the corresponding energy (E), can be calculated via a Rayleigh-Ritz variational procedure. For the trial wave function, Ψ, we take [28]

$$\Psi(\vec{r}_e, \vec{r}_h) = N\,\Upsilon(\rho_e, \rho_h, z_e, z_h)\,e^{-\alpha\rho - \beta(z_e - z_h)^2}, \quad (5)$$

where N is the normalization constant, α and β are variational parameters, and $\Upsilon(\rho_e, \rho_h, z_e, z_h) = F(\rho_e)\,F(\rho_h)\,g(z_e)\,g(z_h)$ is the eigenfunction of the Hamiltonian in equation (1) without the Coulomb term at the right hand side. The noncorrelated radial wavefunctions for single particles are given by

$$F(\rho_i) = J_0(\theta_0\,\rho_i/R), \quad (6)$$

where J_0 is the Bessel function of zero order and $\theta_0 = 2.4048$ is its first zero.

The way of obtaining the noncorrelated axial wavefunctions for single particles relies in a method developed by Xia and Fan [36], which was posteriorly used in the calculation of optical absorption in superlattices under magnetic fields by de Dios Leyva and Galindo [37]. Such an approach is based on the expansion of the electron (hole) states over a complete orthogonal basis of sine functions associated with a QW of infinite potential barriers which width in this work is taken to be $L_\infty = 50$ nm. Consequently, the z_i-dependent eigenfunctions of the Hamiltonian in equation (1) without the Coulomb potential term are written as

$$g(z_i) = \left(\frac{2}{L_\infty}\right)^{\frac{1}{2}} \sum_{n=1}^{\infty} C_n \sin\left(\frac{n\,\pi\,z_i}{L_\infty} + \frac{n\,\pi}{2}\right). \quad (7)$$

Of course, the number of terms included in the calculation cannot be infinite. The convergence of equation (7), for the specific height of the QD considered, is ensured until 10^{-3} meV with the incorporation of 200 terms in the expansion of the $g(z_i)$ wavefunctions.

The trial wavefunction in equation (5) takes into account the anisotropy of the dot via the two variational parameters. This may be important if one is dealing with different R and L values. It is clear that this trial wave function can not reproduce the proper hydrogen-like 3D exciton wavefunction. Nevertheless, this function is expected to be a fair approximation in both the strong confinement regime as well as in the two-dimensional limit.

The energy of the exciton, E, is obtained after minimizing the Hamiltonian with the trial wave function. The exciton binding energy (E_b) is obtained from the definition

$$E_b = E_0 - E, \quad (8)$$

where E_0 is the eigenvalue associated to $\Upsilon(\rho_e, \rho_h, z_e, z_h)$.

3 Results and discussion

The numerical outcome of the study about the intense laser effects on the exciton binding energy is reported for the case of a GaAs-$Ga_{0.67}Al_{0.33}As$ isolated QD, as a prototypical system. The confining potential barrier configuration chosen for electrons (holes) along the z-direction is obtained from $V_e^z = 0.6\,(1155\,x + 370\,x^2)$ meV, ($V_h^z = 0.4\,(1155\,x + 370\,x^2)$ meV), where x is the aluminum molar fraction in the barrier material. The remaining set of parameters included in the calculations are: $\varepsilon_0 = 12.65$, $m_e^* = 0.067\,m_0$, and $m_h^* = 0.34\,m_0$ (where m_0 is the free electron mass). With this set of parameters, and taking into account that the results presented below are all given in terms of α_0, the following relations fulfill: $\frac{\alpha_{0e}}{\alpha_{0h}} = \frac{m_h^*}{m_e^*} \approx 5$, $\alpha_{0e} \approx \frac{5}{6}\alpha_0$, and $\alpha_{0h} \approx \frac{1}{6}\alpha_0$.

It is well known that the classical envelope function approach and effective mass approximation do not work well when the confining potential energy does not change slowly enough [38–40], although there are more recent versions of the model that justify their use even for the abrupt interfaces case [41–43]. In the present work our main assumption is that the confining potential energy is a slowly varying function on the atomic length scale and for this reason in our calculation we avoid to consider too small dimensions of the heterostructure. Consequently, in our calculations the minimum value of both the radius and height of the cylindrical dot we have considered is 3 nm. These values of dimensions of the heterostructure are larger than 5 times the typical lattice constant in the GaAs compounds.

In Figure 2 we present the binding energy of a heavy-hole exciton in the system under study, as a function of the ILF-parameter, for several values of the height of the dot (a) and several values of the applied electric field (b). We observe that the binding energy is a decreasing function of the ILF-parameter. Such a behavior becomes more noticeable for $\alpha_{0e} = \frac{\mu}{m_e^*}\,\alpha_0 < L/2$. Starting from that value of α_{0e} the curve representing the binding energy exhibits a smoother character (notice that near $\alpha_{0e} = L/2$ the curves shown have an inflexion point). In the first regime, the binding energy decreases despite of the reduction in the effective quantum well width, both for electrons and holes (notice that in the regime of $\alpha_{0i} < L/2$, the effective width of the quantum well is $L - 2\alpha_{0i}$). This, in first instance would lead to an increase in the exciton binding energy. However, the reason of the decrease lies in the fact that the two laser-induced Coulomb line centers are moving away of the region in which the carrier density of probability is a maximum, $z_e = z_h = 0$ (see Eq. (4) and the lines I and II depicted in Fig. 2c).

When $\alpha_{0e} > L/2$, the binding energy keeps its decreasing variation. Now, this is a result of the increase of the effective well width (it grows as $L + 2\,\alpha_{0e}$) for the electrons; together with the reduction in the confining potential barrier height since the potential well bottom shifts upwards in energy. This effect is not significant in the case of holes because the variations induced on the width of the potential well that confine them are modulated by a factor of

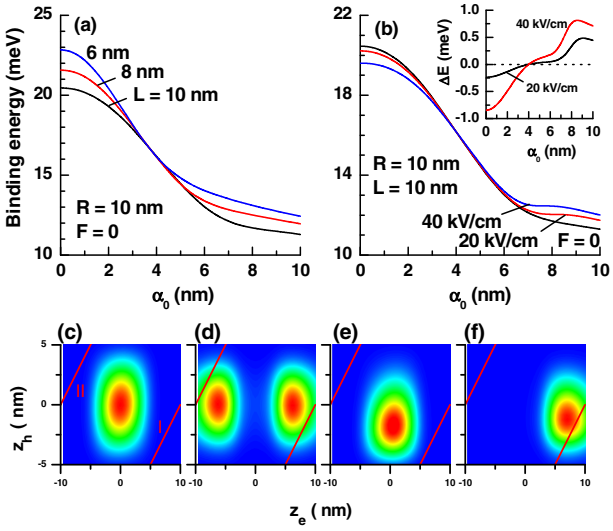

Fig. 2. (Color online) Binding energy of heavy-hole exciton in a GaAs-$Ga_{0.67}Al_{0.33}As$ QD as a function of the ILF-parameter, for several values of the height of the dot (a) and several values of the applied electric field (b). In (a) the results are for $R =$ 10 nm with $F = 0$ whereas in (b) are for $R = 10$ nm with $L = 10$ nm. The inset in (b) shows the shift in the binding energy ($\Delta E(F) = E_b(F) - E_b(F = 0)$). The exciton amplitude of probability in the plane $z_e - z_h$ for $\rho = 0$, $R = 10$ nm, and $L = 10$ nm is also shown under the following conditions: $F = 0$ with $\alpha_0 = 0$ (c); $F = 0$ with $\alpha_0 = 10$ nm (d); $F = 40$ kV/cm with $\alpha_0 = 0$ (e); $F = 40$ kV/cm with $\alpha_0 = 10$ nm (f). In (c) the line I corresponds to the line of Coulomb centers localized along the condition $z_e - z_h - \alpha_0 = 0$ whereas the line II corresponds to the condition $z_e - z_h + \alpha_0 = 0$.

m_e/m_h. The maximum value of the ILF-parameter considered in this work is $\alpha_0 = 10$ nm. It is equivalent to $\alpha_{0e} = 8.3$ nm and $\alpha_{0h} = 1.7$ nm. This means that under no circumstance we can observe in this work changes in the height of the hole-confining potential barrier.

The explanation for the not so steeped decrease of the heavy-hole exciton binding energy when $\alpha_{0e} > L/2$, compared with the above discussed situation is the following. In that case, there will be a modification in the potential profile configuration, associated with the larger value of the ILF-parameter. This change appears in the form of a double quantum well in the z_e-direction (see Fig. 2d). This makes that the positions of the two maxima of the electron density of probability are now close to the Coulombic center lines I and II. That is, the double quantum well configuration induces a spatially indirect exciton system, which favors the enhancement of the Coulomb interaction. Nonetheless, the dominant effect continues to be that of the geometric confinement and, therefore, the binding energy definitively decreases.

By comparing the different curves in Figure 2a one may observe that there is an increase of the binding energy as long as the quantum dot's height diminishes. In the situation when $\alpha_{0e} < L/2$, this energy becomes larger when form smaller L given the associated rise in the degree of carrier localization around $z_e = z_h = 0$. This has the

consequence of the enhancement of the electron and hole wavefunction overlapping, thus causing the strengthening of the Coulombic interaction (there will be a reduction in the expected value of the axial electron-hole distance). On the other hand, in the regime in which $\alpha_{0e} > L/2$, E_b also augments. In this case of indirect excitonic configuration, the decrease in the dot's height makes the two maxima of the electron density of probability to be displaced towards the region around $z_e = 0$. It is precisely there where the maximum of the hole density of probability locates ($z_h = 0$). This reflects in the increase of the wavefunctions overlap and, consequently, the carriers correlation. However, it can be seen that, when α_{0e} is of the order of $L/2$, the binding energy is essentially independent of the dot's height. The reason for this lies in the fact that, in such a limit, the wavefunction is mostly confined within a quasi-delta-like potential well, with only very few information about the height of the QD.

It is possible to observe a mixed behavior of the exciton binding energy when there is an applied electric field (see Fig. 2b). If $\alpha_{0e} < L/2$, E_b decreases as a result of the field-induced polarization of the electron-hole system. This makes the effective distance between the two carriers to become larger. Thus, the strength of the Coulombic interaction diminishes, with the consequent reduction in the magnitude of the binding energy. In the situation when $\alpha_{0e} > L/2$ – in which we detect the presence of an indirect exciton, given the ILF-induced double well configuration for electrons – the presence of an electric field favors the shift of the electron wavefunction towards $z_e > 0$. In addition, the electron becomes confined within a narrower spatial region, augmenting its degree of localization.

Well then, the electron will now pass from having two maxima of its density of probability to a single one. In other words, there will be an enhancement of the Coulombic interaction with the hole and, therefore, the heavy exciton binding energy increases. An additional argument in favor of the increment of E_b in this situation can be provided by observing Figure 2f. Notice that the electric field positively contributes to the shift of the probability density maximum towards the Coulomb center line labeled as I in the figure. This, in other words, implies an increase of both the Coulombic interaction and exciton binding energy. The inset in Figure 2b shows that the three curves essentially have the same binding energy at $\alpha_0 \sim 4$ nm. This corresponds, approximately, to the transition from direct to indirect exciton regimes, for the particular geometry chosen in Figure 2b.

In Figure 3 there are depicted our results for the binding energy of heavy-hole exciton in a GaAs-$Ga_{0.67}Al_{0.33}As$ QD as a function of the radius of the dot (a) and of the height of the dot (b) for several values of the ILF-parameter. One can observe from Figure 3a that the exciton binding energy monotonically decreases as long as the dot's radius augments. This is due to the loss of confinement over the radial part of the carrier wavefunctions. It is clear that, for large enough values of the radius, our results will converge exactly to those corresponding to a finite barrier quantum well. Notice that the greater

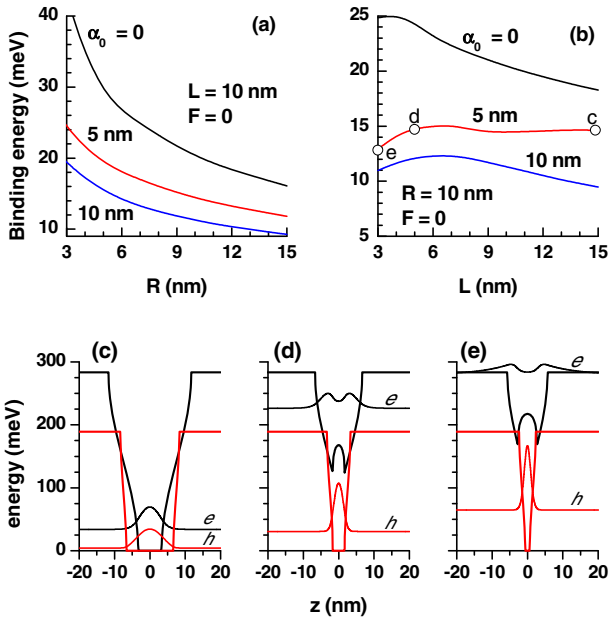

Fig. 3. (Color online) Binding energy of heavy-hole exciton in a GaAs-$Ga_{0.67}Al_{0.33}As$ QD as a function of the radius of the dot (a) and of the height of the dot (b) for several values of the ILF-parameter. The results are for zero applied electric field with $L = 10$ nm (a) and $R = 10$ nm (b). In (c), (d), (e) are shown the z-dependent confinement potential and the amplitude of probability for the ground state both for electrons (e) and holes (h) considering for the geometry of the structure those denoted by open dots in (b).

effects come from the variation of the dot's radius are those appearing in the situation in which $\alpha_0 = 0$ for the value $L = 10$ nm. In this case, the exciton wavefunction is strongly confined in the axial direction. In the cases of $\alpha_0 = 5$ nm and $\alpha_0 = 10$ nm, the effective height of the QD is of the order of 20 nm and 30 nm, respectively. This means that such size is two or three times larger than the effective Bohr radius in the GaAs. Therefore, the system will have a very low degree of axial confinement, which explains the quasi-parallel variation of the corresponding binding energy curves. It is worth mentioning that our curve for $\alpha_0 = 0$ is in perfect agreement with results previously reported in GaAs-based cylindrical QDs [28].

From Figure 3b one observes that for $\alpha_0 = 0$ the value of the binding energy grows, until reaching a maximum, as long as the QD height diminishes. With the reduction in the dot's height, the electron wavefunction tends to localize near $z_e = z_h = 0$. Then, the expected value of the electron-hole distance becomes smaller and the Coulombic interaction strengthens, with the consequent increase of E_b. It comes a time when the height of the dot reaches a value small enough to allow – together with the effect of the finite confining barriers – the electron wavefunction to spread into the barrier regions.

Let us discuss now what happens in the cases represented by the curves with $\alpha_0 = 5$ nm and $\alpha_0 = 10$ nm. Particularly, we are going to analyze the curve of $\alpha_0 = 5$ nm, in which three points have been marked. They correspond

to the confining potentials and electron and hole densities of probability shown in Figures 3c–3e. Going from $L = 15\,\text{nm}$ to $L = 5\,\text{nm}$, it can be observed that there is an increase in the hole localization in the region around $z_e = z_h = 0$, with the appearance of a configuration with two coupled quantum dots in the case of the electrons. The effective width of the structure, for electrons, decreases as well. This could lead us to expect that the higher degree of localization in their wavefunctions, will lead to larger values of the binding energy.

But, indeed, given the creation of an indirect exciton, there is, in this case, an effective increase of the electron-hole distance, with the associated reduction in E_b. The sum of these two opposite effects will result in the almost constant behavior observed in the curve, when the dot's height goes from $L = 15\,\text{nm}$ to $L = 5\,\text{nm}$.

Now, by going further down in the value of the QD height, when we get to $L = 3\,\text{nm}$ it is seen that the effect of the ILF entails a strong delocalization of the electron. This makes that its energy practically equals that of the potential well height. Under such a condition, the axial distance between the two kinds of carriers substantially increases, and the Coulombic interaction between them is strongly reduced. The consequence of this is the fall in the exciton binding energy that can be noticed in the curve discussed. In the case of a laser-field parameter $\alpha_0 = 10\,\text{nm}$, the behavior of the binding energy curve is explained in terms of the same arguments used above when discussing the $\alpha_0 = 5$ nm one. By extending the calculations beyond $L = 20\,\text{nm}$, the curve for $\alpha_0 = 10\,\text{nm}$ acquires the same character shown by the curve that corresponds to $\alpha_0 = 5\,\text{nm}$.

We present in Figure 4 our results for the shift in the binding energy ($\Delta E(F) = E_b(F) - E_b(F = 0)$) of a heavy-hole exciton in a GaAs-$Ga_{0.67}Al_{0.33}As$ QD as a function of the applied electric field for several values of the ILF-parameter. As it is known, this quantity is related with the energy position of the exciton-related photoluminescence peak (the so-called PL_{peak}). By analyzing the graphics in the figure, and in accordance with the results shown in Figure 2a, one may observe the following features:

1. When $\alpha_0 = 0$ the binding energy decreases as long as the strength of the applied field augments, due to polarization that it induces over the electron-hole pair. This decreasing behavior of E_b contributes to the blueshift in the energy of the exciton-related photoluminescence peak.
2. For $\alpha_0 = 5\,\text{nm}$ the binding energy is essentially constant. This situation corresponds to the crossing of the curves in Figure 2b; which is due to the transition between the direct and indirect exciton regimes. Then, the shift line is almost constant.
3. If $\alpha_0 = 10\,\text{nm}$, the binding energy augments despite that there is now a configuration of coupled double quantum dot. This happens because the electric field favors that it will only appear a single maximum in the density of probability of the exciton, which locates within the region $z_e > 0$, near the line of Coulomb centers parameterized by the condition $z_e - z_h - \alpha_0 = 0$, as can be seen from the Figures 4c and 4d and in Figure 2f. In this case, the effect of the electric field translates into the favoring of the electrostatic interaction through a single line of Coulomb centers localized in the region $z_e > 0$, with all the electronic density of probability concentrated around it. In the case of the line of Coulomb centers located in the region $z_e < 0$ ($z_e - z_h + \alpha_0 = 0$), the wavefunctions of the electron and the hole are practically null and, consequently, such a line of charged centers does not participate in the electrostatic interaction. This increasing behavior of the binding energy leads now to the redshift of the luminescence peak energy.

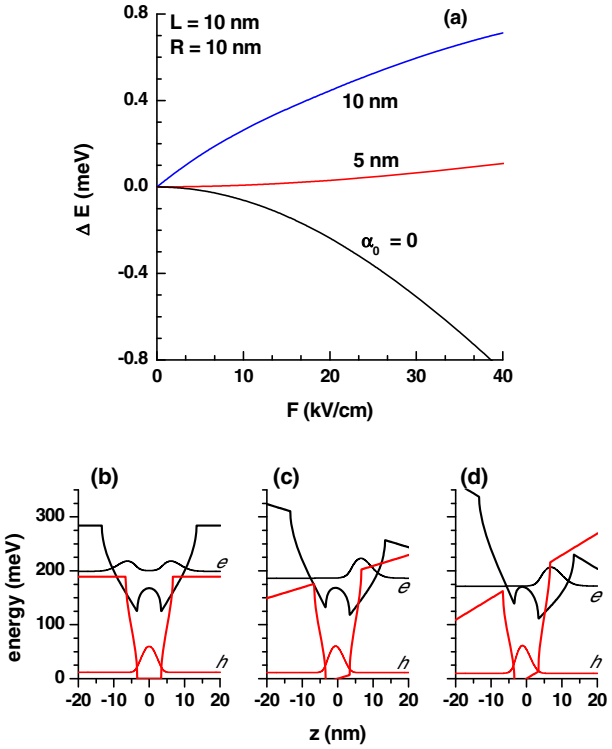

Fig. 4. (Color online) (a) Shift in the binding energy ($\Delta E(F) = E_b(F) - E_b(F = 0)$) of heavy-hole exciton in a GaAs-$Ga_{0.67}Al_{0.33}As$ QD as a function of the applied electric field for several values of the ILF-parameter. The results are for $L = 10$ nm with $R = 10$ nm. In (b), (c), (d) are shown the z-dependent confinement potential and the amplitude of probability for the ground state both for electrons (e) and holes (h) for the same dimensions of the dot as in (a) but for $\alpha_0 = 10$ nm. Three values of the applied electric field have been considered: zero (b), $F = 20$ kV/cm (c), and $F = 40$ kV/cm (d).

On the other hand, Figure 5 shows our results for the expectation value of the in-plane (ρ_{eh}) and axial (z_{eh}) electron-hole distance of heavy-hole exciton in a GaAs-$Ga_{0.67}Al_{0.33}As$ QD as a function of the ILF-parameter. One may clearly observe that the most significant changes associated with the ILF-parameter are those occurring in z_{eh}.

In a structure with $R = 10\,\text{nm}$ and average height of $L = 8\,\text{nm}$, a change in the ILF-parameter that amounts

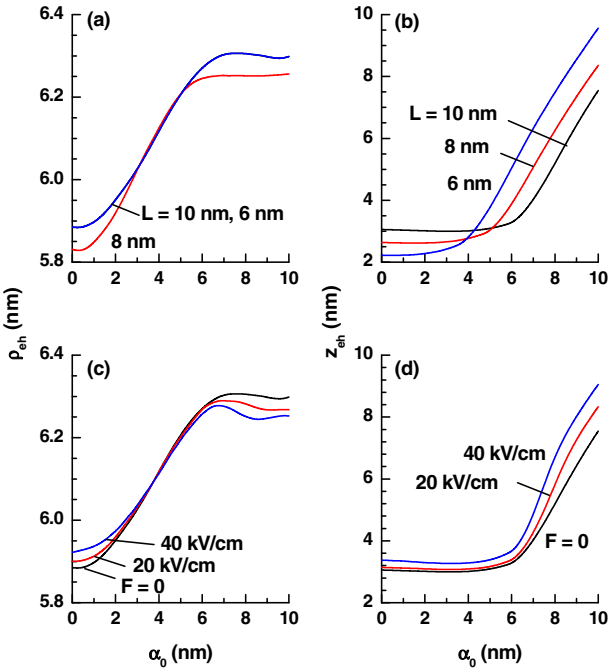

Fig. 5. (Color online) Expectation value of the in-plane (left hand panel) and axial (right hand panel) electron-hole distance of heavy-hole exciton in a GaAs-$Ga_{0.67}Al_{0.33}As$ QD as a function of the ILF-parameter. In (a) and (b) the results are for $R = 10$ nm and $F = 0$, whereas in (c) and (d) the results are for $R = 10$ nm and $L = 10$ nm.

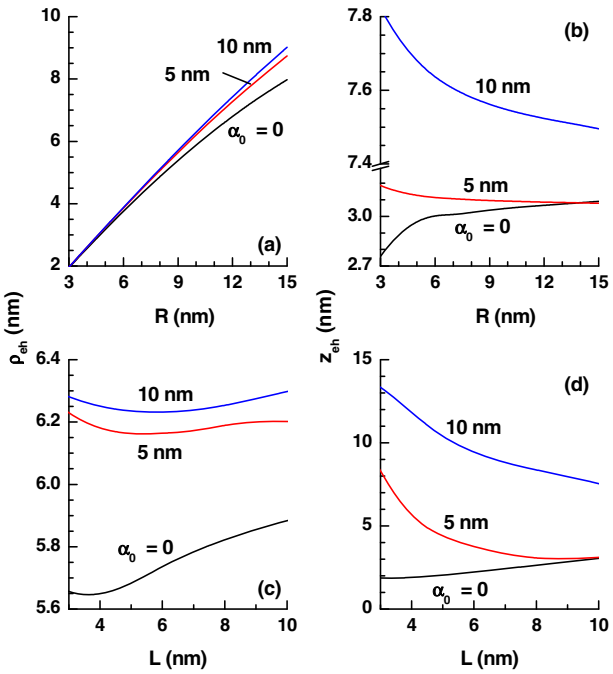

Fig. 6. (Color online) Expectation value of the in-plane (left hand panel) and axial (right hand panel) electron-hole distance of heavy-hole exciton in a GaAs-$Ga_{0.67}Al_{0.33}As$ QD with zero applied electric field and as a function of the radius of the dot (a, b) and as a function of the height of the dot (c, d). In (a, b) the results are for $L = 10$ nm whereas in and (c, d) are for $R = 10$ nm.

10 nm in value will imply an increase in ρ_{eh} of only 0.4 nm, approximately. Whereas, in the case of z_{eh} there will be an increase which ranks between 4.5 nm and 7.3 nm. Its is possible to observe from Figures 5a and 5c that as soon as the ILF-parameter differs from zero, there will be a growth in the value of ρ_{eh}. The reason for this is that, when $\alpha_0 < L/2$, a nonzero value of the ILF-parameter implies an axial compression of the wavefunction, leading to a larger extension of it along the radial direction (notice that this wavefunction is normalized to unity). Within the same regime for α_0, in Figures 5b and 5d we can observe that a growth in the value of the ILF-parameter leaves almost without change the value of z_{eh}. This can be understood in relation with several aspects: (1) the strong localization of the hole wavefunction around $z_h = 0$; (2) the weak influence of the ILF-parameter on the width of the potential that confines the holes in the system; and (3) the effect of compensation generated by the increase in the width of the quantum well for the electrons, which grows as a function of the laser parameter in the form $L + 2\,\alpha_{0e}$. The quasi-constant behavior of z_{eh} and the increasing one of ρ_{eh}, in the $\alpha_0 < L/2$ regime of the laser field, can be clearly identified with the presence of spatially direct excitons. This means that both electrons and holes localize within the same spatial region. Notice that above the limit $\alpha_0 = L/2$ the value of ρ_{eh} is practically constant and, instead, z_{eh} is an increasing function of the ILF-parameter. In keeping with the results shown in Figures 3b–3d, when $\alpha_0 > L/2$ a double quantum well profile is induced in the case of the conduction band whilst the configuration of single quantum well is kept in the case of the valence band profile. This reflects in an increase of the axial distance between the carriers, (z_{eh}), which grows as long as the central potential barrier that uncouples the two wells for the electrons augments. A linear increase of z_{eh}, or a constant behavior in ρ_{eh} as a result of the increase in the value of the ILF-parameter, clearly corresponds to the situation of spatially indirect excitons. The crossing of the different curves in Figure 5b is explained by the dependence of the value of α_0 at which the direct-to-indirect exciton transition takes place on the height of the QD. Notice that as long as the value of L is becoming smaller, the value of α_0 that corresponds to the direct-to-indirect transition for the exciton simultaneously decreases. For instance, when $L = 10$ nm the transition occurs approximately at $\alpha_0 = 6$ nm; but if $L = 6$ nm this happens for $\alpha_0 = 3$ nm.

In Figure 6 we present our results for the expectation value of the in-plane and axial electron-hole distance of heavy-hole exciton in a GaAs-$Ga_{0.67}Al_{0.33}As$ QD with zero DC applied electric field and as a function of the radius of the dot (a, b) and as a function of the height of the dot (c, d), for several values of the ILF strength.

From Figure 6a it is seen that ρ_{eh} is always an increasing function of R, with only very slight modifications coming from the variations in the ILF-parameter. This dependence is a clear indication that, up to the

value $R = 15$ nm, the excitonic wavefunction is – all the time – under the influence of the in-plane confinement. Nonetheless, it is a fact that, for large enough values of the dot's radius, there must be an asymptotic behavior of the ρ_{eh} curves, with different approaching limits that depend on the quantum well width and the value of the ILF-parameter used.

We can observe, in Figure 6b, the little influence that an increase in the dot's radius has over the axial expected distance between the two carriers. A variation of 12 nm in R will result, only, in changes in the range of 0.3 nm-0.5 nm in z_{eh}. Notice the asymptotic character acquired by the curves of z_{eh} for radii larger than ∼15 nm. For the sake of comparison, the expected value of the electron-hole distance in a hydrogen-like complex in bulk is of $1.5a_0^*$, where a_0^* is the effective Bohr radius. In the GaAs, $a_0^* = 11.9$ nm if it is defined using the reduced effective mass of the electron-hole pair. Then, it becomes clear that, for $R = 15$ nm, the size of the quantum dot is close to reach the dimensions at which the exciton wavefunction starts losing the information about the presence of confining potential barriers.

In Figures 6c and 6d, one detects that a change of 7 nm in the height of the QD leads only to variations of 0.3 nm in ρ_{eh} at the time that induces changes in z_{eh} that rank between 2 and 7 nm, depending on the value of the ILF-parameter used. The systematically decreasing behavior in z_{eh} for $\alpha_0 = 0$ as L decreases is explained by the fact that the exciton wavefunction goes from being confined in a QD of radius R and height equals to L, to confine itself within a QD of radius R and height L_∞; with a large part of the electronic wavefunction localized into the barrier regions. The decreasing variation of the curves of $\alpha_0 = 5$ nm and 10 nm in Figure 6d, for growing L, is due to the localization of the wavefunction in the region of the quantum well. The maximum observed in the curve for $\alpha_0 = 10$ nm appears exactly at the value of the well width for which there occurs the transition between two maxima to a single maximum in the hole amplitude of probability.

Figure 7 shows the normalized $\mathrm{PL_{peak}}$ energy transition of heavy-hole exciton in a GaAs-$Ga_{0.67}Al_{0.33}As$ QD as a function of the ILF-parameter, for several values of the height of the dot and several values of the applied electric field. As an additional information, the oscillator strengths are also depicted in the insets.

The $\mathrm{PL_{peak}}$ is obtained by means of the expression $\mathrm{PL_{peak}} = E_0^e + E_0^h + E_g - E_b$; where E_0^e and E_0^h are, respectively, the energies of the lowest confined states of the electron and the hole. Besides, E_g is the energy of the gap in the GaAs. The term normalized $\mathrm{PL_{peak}}$ means that we are referring the $\mathrm{PL_{peak}}$ with respect to the GaAs energy gap. In other words, we are considering the quantity $\mathrm{PL_{peak}} - E_g$. All the curves show that the normalized $\mathrm{PL_{peak}}$ is an growing function of the ILF-parameter. This is basically associated with the increase of E_0^e because, for the values of α_0 considered, the hole well width does not exhibit substantial modifications. In each curve we are able to detect to well-defined regimes. When $\alpha_0 \lesssim L/2$ the curves are convex, and when $\alpha_0 \gtrsim L/2$ they become

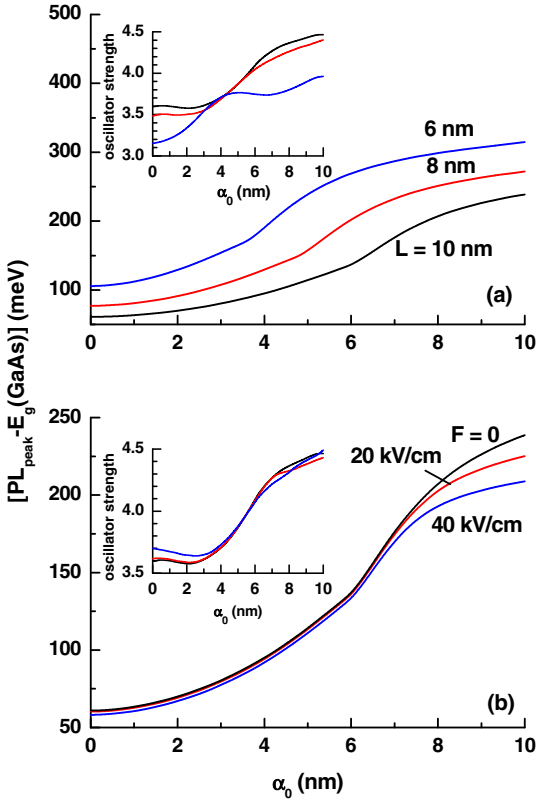

Fig. 7. (Color online) Normalized $\mathrm{PL_{peak}}$ energy transition of heavy-hole exciton in a GaAs-$Ga_{0.67}Al_{0.33}As$ QD as a function of the ILF-parameter, for several values of the height of the dot (a) and several values of the applied electric field (b). In (a) the results are for $R = 10$ nm with $F = 0$ whereas in (b) are for $R = 10$ nm with $L = 10$ nm. The insets depict the corresponding oscillator strength.

concave. In the first case, we explain the curvature by the fact that the energy of the electron grows with respect to the bottom of its confining potential well, and also because the rather abrupt decrease of the binding energy (see Fig. 2). In the second case, we have the system in the regime of spatially indirect excitons. Here, the increase in the normalized $\mathrm{PL_{peak}}$ is a consequence of the shift of the conduction band confining well bottom towards higher energies. In this situation, the variations of E_0^e with respect to the bottom of its respective potential well are almost imperceptible. Additionally, one should take into account that, in this regime, the binding energy decreases; but this happens at a lower rate if compared with the first regime discussed (see again Fig. 2).

The oscillator strength, shown in the corresponding insets, augments in all cases. That behavior is essentially due to the decreasing character of the binding energy, which is the second term in the denominator that appears in the definition of this quantity.

Finally, in Figure 8 we are presenting the calculated results for the normalized $\mathrm{PL_{peak}}$ associated to heavy-hole excitons in a GaAs-$Ga_{0.67}Al_{0.33}As$ QD as a function of the radius of the dot and of the height of the dot, for several values of the ILF-parameter.

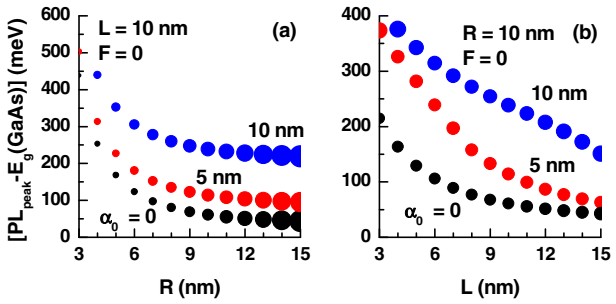

Fig. 8. (Color online) Normalized $\mathrm{PL_{peak}}$ of heavy-hole exciton in a GaAs-$Ga_{0.67}Al_{0.33}As$ QD as a function of the radius of the dot (a) and of the height of the dot (b) for several values of the ILF-parameter. The results are for zero applied electric field with $L = 10$ nm (a) and $R = 10$ nm (b). The area of the dots is proportional to the oscillator strength.

It can be noticed that, as a general trend, the normalized $\mathrm{PL_{peak}}$ decreases as long as the size of the structure augments. This is basically due to the diminishing in E_0^e and E_0^h, given the loss in carrier localization. In Figure 8b we see that the normalized $\mathrm{PL_{peak}}$ has a more complex behavior if compared to that shown in Figure 8a. This fact is mostly associated with the form exhibited by the binding energy, as can be seen when comparing Figures 2a and 2b.

4 Conclusions

In the article, the properties of heavy-hole excitons in GaAs-$Ga_{1-x}Al_xAs$ quantum dots under intense laser and applied dc electric fields are studied for a set of different values of the fields intensities and the dot spatial dimensions. Special attention is paid to the laser-field-induced spatially direct-indirect exciton transition.

We have obtained that, as an overall behavior, the exciton binding energy is a decreasing function of the laser field strength, with and without the presence of an additional applied DC electric field. The reason behind this feature is the reduction in the strength of the Coulombic electron-hole interaction that associates mostly with the growth in the expected electron-hole distance along the quantum dot's axial direction. In relation with this, the decrease mentioned is more pronounced in the situation of larger values if the dot's height.

The shift in the exciton binding energy as a function of the applied DC field is a decreasing function of the field strength in the case of zero laser field. However, this quantity turns out to exhibit an increasing variation when there is an intense laser field applied. This fact is a direct consequence of the spatially indirect regime of the exciton, related with both the DC-field-induced carrier polarization as well as the laser-induced transition to a coupled double quantum well potential profile in the conduction band.

Following mainly the behavior of the binding energy, the reported exciton-related normalized photoluminescence peak energy shows an increasing behavior as a function of the intense laser field strength, for a fixed geometry of the quantum dot. However, for a fixed value of the intense laser field parameter, this quantity reveals to have a decreasing dependence on both the dot's height and radius.

Our results reveal that for the system studied here the influence of the electric field on the exciton binding energy is rather small (less than 2 meV). Previous reports show that the effect of the $\Gamma - X$ crossover induced by the application of hydrostatic pressure to the system, or the presence of a magnetic field are more successful in attaining larger corrections to this quantity [44–46]. A study on the combined influences of ILF, applied magnetic field, and hydrostatic pressure on the properties of electrons and excitons confined in cylindrical shaped QD with parabolic lateral confinement potential is currently carried out and will be published elsewhere.

Finally, it is important to comment that our work has been based on the analysis of the ground state, only, either for electrons or for holes. However, as the well width becomes larger and as the internal soft barrier increases, the system will be eventually transformed from being a single QD to that consisting of two separated QD [47]; during this transition, the difference between the eigenenergies of the ground state and the first excited state gradually decreases. Hence there certainly is a limit to the applicability of the present method in the situation of wide QDs.

MEMR acknowledges support from Mexican CONACYT through grant CB-2008-101777. This research was partially supported by Colombian Agencies: CODI-Universidad de Antioquia (project: E01553-Propiedades ópticas no lineales en heteroestructuras semiconductoras de baja dimensionalidad (nitruros y arseniuros)) and Facultad de Ciencias Exactas y Naturales-Universidad de Antioquia (CAD-exclusive dedication project 2012-2013). MEMR and CAD thank CONACYT (Mexico) and COLCIENCIAS (Colombia) for support under the 2012-2013 Bilateral Agreement "Estudio de propiedades ópticas, electrónicas y de transporte en sistemas de baja dimensión basados en carbono y semiconductores III-V: efectos de campos externos, temperatura y presión hidrostática". The work was developed with the help of CENAPAD-SP, Brazil. The authors are grateful to The Scientific and Technological Research Council of Turkey (TÜBİTAK) for a research grant (TÜBİTAK 109T650).

References

1. C. Weisbuch, B. Vinter, *Quantum Semiconductor Structures: Fundamentals and Applications* (Academic Press, London, 1991)
2. K. Goser, P. Glosekotter, J. Dienstuhl, *Nanoelectronics and Nanosystems: From Transistors to Molecular and Quantum Devices* (Springer-Verlag, New York, 2004)
3. S.D. Ganichev, W. Prettl, *Intense Terahertz Excitation of Semiconductors* (Oxford University Press, Oxford, 2006)
4. A.P. Jauho, K. Johnsen, Phys. Rev. Lett. **76**, 4576 (1996)
5. W. Xu, Europhys. Lett. **40**, 411 (1997)

6. B.G. Enders, F.M.S. Lima, O.A.C. Nunes, A.L.A. Fonseca, D.A. Agrello, Q. Fanyao, E.F. Da Silva Jr., V.N. Freire, Phys. Rev. B **70**, 035307 (2004)
7. R.G. Mani, J.H. Smet, K. von Klitzing, V. Narayanamurti, W.B. Johnson, V. Umansky, Nature **420**, 646 (2002)
8. N.G. Asmar, A.G. Markelz, E.G. Gwinn, J. Cerne, M.S. Sherwin, K.L. Campman, P.F. Hopkins, A.C. Gossard, Phys. Rev. B **51**, 18041 (1995)
9. H. Hsu, L.E. Reichl, Phys. Rev. B **74**, 115406 (2006)
10. L.C.M. Miranda, J. Phys. C: Solid State Phys. **9**, 2971 (1976)
11. O.A.C. Nunes, Solid State Commun. **45**, 53 (1983)
12. R.M.O. Galvao, L.C.M. Miranda, Phys. Rev. B **28**, 3593 (1983)
13. J.W. Sakai, O.A.C. Nunes, Solid State Commun. **64**, 1393 (1987)
14. H.S. Brandi, A. Latgé, L.E. Oliveira, Phys. Stat. Sol. B **210**, 671 (1998)
15. H.S. Brandi, A. Latgé, L.E. Oliveira, Phys. Rev. B **70**, 153303 (2004)
16. E.C. Niculescu, L.M. Burileanu, J. Optoelectron. Adv. Mater. **9**, 2713 (2007)
17. F.E. López, E. Reyes-Gómez, H.S. Brandi, N. Porras-Montenegro, L.E. Oliveira, J. Phys. D **42**, 115304 (2009)
18. E.C. Niculescu, L.M. Burileanu, A. Radu, Superlatt. Microstruct. **44**, 173 (2008)
19. E.C. Niculescu, A. Radu, M. Stafe, Superlatt. Microstruct. **46**, 443 (2009)
20. A.J. Peter, Phys. Lett. A **374**, 2170 (2010)
21. L.M. Burileanu, A. Radu, Opt. Commun. **284**, 2050 (2011)
22. E.C. Niculescu, L.M. Burileanu, A. Radu, A. Lupescu, J. Lumin. **121**, 1113 (2011)
23. F.M.S. Lima, M.A. Amato, O.A.C. Nunes, A.L.A. Fonseca, B.G. Enders, E.F. da Silva Jr., J. Appl. Phys. **105**, 123111 (2009)
24. E. Kasapoglu, H. Sari, U. Yesilgul, I. Sökmen, J. Phys.: Condens. Matter **18**, 6263 (2006)
25. M. Santhi, A. John Peter, Eur. Phys. J. B **71**, 225 (2009)
26. C.A. Duque, E. Kasapoglu, S. Şakiroglu, H. Sari, I. Sökmen, Appl. Surf. Sci. **256**, 7406 (2010)
27. N. Eseanu, Phys. Lett. A **374**, 1278 (2010)
28. S. Le Goff, B. Stébé, Phys. Rev. B **47**, 1383 (1993)
29. M. Gavrila, J.Z. Kaminski, Phys. Rev. Lett. **52**, 613 (1984)
30. M. Pont, N.R. Walet, M. Gavrila, C.W. McCurdy, Phys. Rev. Lett. **61**, 939 (1988)
31. H. Sari, E. Kasapoglu, I. Sökmen, Phys. Lett. A **311**, 60 (2003)
32. E. Kasapoglu, H. Sari, M. Güneş, I. Sökmen, Surf. Rev. Lett. **11**, 403 (2004)
33. E. Kasapoglu, I. Sökmen, Physica B **403**, 3746 (2008)
34. O.O. Diniz Neto, Fanyao Qu, Superlatt. Microstruct. **35**, 1 (2004)
35. N. Eseanu, Phys. Lett. A **375**, 1036 (2011)
36. J.-B. Xia, W.-J. Fan, Phys. Rev. B **40**, 8508 (1989)
37. M. de Dios Leyva, V. Galindo, Phys. Rev. B **48**, 4516 (1993)
38. J.C. Slater, Phys. Rev. **76**, 1592 (1949)
39. D.J. BenDaniel, C.B. Duke, Phys. Rev. **152**, 683 (1966)
40. N.W. Ashcroft, N.D. Mermin, *Solid State Physics* (Holt, Rinehart, Winston, New York, 1976)
41. M.G. Burt, J. Phys.: Condens. Matter **4**, 6651 (1992)
42. M.G. Burt, Phys. Rev. B **50**, 7518 (1994)
43. B.A. Foreman, Phys. Rev. B **52**, 12241 (1995)
44. Z. Xiao, J. Appl. Phys. **86**, 4509 (1999)
45. W. Xie, Physica B **315**, 240 (2002)
46. K.L. Janssens, F.M. Peeters, V.A. Schweigert, Phys. Rev. B **63**, 205311 (2011)
47. C.D. Simserides, G.P. Triberis, J. Phys.: Condens. Matter **5**, 6437 (1993)